Journal of King Saud University – Science 31 (2019) 352–361

Contents lists available at ScienceDirect

Journal of King Saud University – Science

journal homepage: www.sciencedirect.com

Original article

Entropy generation due to mixed convection over vertical permeable cylinders using nanofluids

Sameh E. Ahmed [a,*], Z.A.S. Raizah [b], Abdelraheem M. Aly [a]

[a] Department of Mathematics, Faculty of Science, South Valley University, Qena, Egypt
[b] Department of Mathematics, Faculty of Science for Girls, Abha, King Khalid University, Saudi Arabia

ARTICLE INFO

Article history:
Received 28 May 2017
Accepted 29 July 2017
Available online 3 August 2017

Keywords:
Boundary layer
Mixed convection
Vertical cylinder
Entropy generation
Nanofluid

ABSTRACT

This paper discusses the thermal stratification and suction/injection effects on the entropy generation and heat transfer due to convective boundary layer flow over a vertical stretching cylinder using Buongiorno's model for nanofluids. For the nanoparticle volume fraction, the boundary conditions are taken such that its normal fluxes are zero. The governing equations and the entropy equation are derived in cylindrical coordinates, in details. Similar transformations are used to convert the governing equation into ordinary differential equations and the resulting system is solved numerically using MATLAB function *bvp4c*. The obtained results are presented in terms of velocity profiles, temperature distributions, nanoparticle volume fraction, local entropy generation, skin friction coefficient and local Nusselt number. It is found that the minimum values of the entropy generation occur in the injection case, while the suction case maximizes the entropy generation. The increase in the thermal stratification parameter decreases the profiles of velocity temperature and nanoparticle volume fraction, while it enhances the entropy generation.

1. Introduction

The study of heat transfer by mixed/natural convection boundary layer flow over stretching cylinders has received considerable attentions due to its great importance in many industrial engineering applications. These applications include, for example, fiber technology, wire drawing, cooling of nuclear reactors during emergency shutdown conditions, extrusion processes, rubber sheets and polymer extrusion, manufacture of plastic and glass–fiber production, etc (Kakaç and Pramuanjaroenkij, 2009). Hence, many researchers were interested in studying this topic. Mansour et al. (2011) discussed the effect of thermal stratification on mixed convection flow of micropolar fluids over a permeable stretching tube. They interested with both strong and weak concentration of microelement cases. Their results indicated that the increase in thermal stratification parameter causes enhancements in the rate of heat transfer. Ahmed et al. (2014) focused on the presence of heat generation/absorption effect in the flow region of nanofluid flow over stretching cylinder. It is found that the increase in the solid volume fraction has a dominant effect on the local Nusselt number for all models under consideration. Grosan and Pop (2011) reported on the boundary layer flow of a nanofluid past a vertical tube with stagnation point. They indicated that there exist dual solutions when the tube surface is cooled. The entropy generation analysis due to boundary layer flow and heat transfer past a hyperbolic stretching cylinder is investigated by Majeed et al. (2016). It is observed that the curvature parameter has dominant effect on the flow and heat transfer characteristics. The results obtained by Mukhopadhyay (2013) show that the increase in magnetic field parameter or slip parameter reduces the velocity profiles. Mukhopadhyay (2012) examined the boundary layer flow and heat transfer past a vertical stretching cylinder saturated in porous media. A similar solutions and a shooting technique were used in the solution of problem. The increase in the curvature parameter is found to has negative effect on the velocity profiles and temperature distributions. Rashad et al. (2013) analyzed mixed convection boundary layer flow over a horizontal cylinder with a stagnation point and embedded in porous medium using nanofluid. The results show that the increase in mixed convection

* Corresponding author.
E-mail addresses: sameh.hassan@sci.svu.edu.eg (S.E. Ahmed), zhbarizah@hotmail.com (Z.A.S. Raizah), abdelreheam.abdallah@sci.svu.edu.eg (A.M. Aly).

Peer review under responsibility of King Saud University.

Production and hosting by Elsevier

http://dx.doi.org/10.1016/j.jksus.2017.07.010
1018-3647/

Nomenclature

Be	Bejan number
Br	Brinkman number
C_f	local skin-friction coefficient
D_B	Brownian diffusion coefficient
D_T	thermophoretic diffusion coefficient
$\boldsymbol{g}$	gravity acceleration vector (m/s^2)
Gr	Grashof number
k	thermal conductivity (W/mK)
Le	Lewis number
n	thermal stratification parameter
Ns	total entropy generation
Nu	local Nusselt number
N_b	Brownian motion parameter
N_t	thermophoresis parameter
Nr	buoyancy ratio
Pr	Prandtl number
Re	Reynolds number
S_T	dimensionless entropy generation due to the heat transfer irreversibility
S'''	Local entropy generation (W/m^3 K)
S_ϕ	entropy generation due to mass diffusion
S_F	entropy generation due to viscous dissipation
T	temperature (K)
$\boldsymbol{u}$	velocity vector (m/s)

Greek symbols

τ	stress tensor
$(\rho C)_p$	heat capacity of the nanoparticle material
ϕ	nanoparticle volume fraction (%)
ρ	density (kg/m^3)
$(\rho C)_f$	heat capacity of the base fluid
γ	suction/injection parameter
Ω	dimensionless temperature difference
Σ	dimensionless concentration difference
ϵ	dimensionless constant
η	similarity variable

Subscripts

f	base fluid
p	nanoparticles
w	surface conditions
∞	ambient conditions

parameter increases the velocity profiles, while it decreases the distributions of temperature and nanoparticle volume fraction. The references (Anwar et al., 2008; Wang, 1988; Ishak et al., 2008; Khan and Pop, 2010; Bachok and Ishak, 2010) discussed the boundary layer flow over cylinders using regular fluid, nanofluid and viscoelastic fluid.

Buongiorno (2006) presented a comprehensive study for heat transfer by convective in nanofluids. In this investigation, the author presented a logical explanation for abnormal increase in heat transfer coefficient for such fluid. He says that the nanofluids properties vary significantly within the boundary layer and this due to the effect of thermophoresis and temperature gradients. Therefore, these effects cause a decrease of viscosity within the boundary layer and consequently the heat transfer is enhanced. Kuznetsov and Nield (2010) used Buongiorno's model to discuss the heat transfer by convective boundary layer flow along a vertical plate via nanofluids. They showed that the heat transfer rate is a decreasing function of buoyancy-ratio parameter, Brownian motion parameter and thermophoresis parameter. Nield and Kuznetsov (2009) used the nanofluid model of Buongiorno (2006) to investigate the Ching-Minkowyze problem for natural convection of a nanofluid along a vertical plate saturated porous medium. They indicated that the thickness of the mass fraction boundary layer is smaller than the thermal boundary layer when Lewis number is greater than 1. Kuznetsov and Nield (2013, 2014) revised the models (Kuznetsov and Nield, 2010; Nield and Kuznetsov, 2009) such that the nanoparticle volume fraction on the wall is passively rather than actively controlled. Elshehabey and Ahmed (2015) discussed the mixed convection of a nanofluid flow in a lid-driven enclosure with non-uniform temperature distributions on both side walls. They used the nanofluid model in Buongiorno (2006) to simulate their problem. They noted that the presence of magnetic force causes a reduction in the nanofluid flow. Ahmed and Mahdy (2016) developed the model in Buongiorno (2006) to discuss the bioconvection flow over a vertical wavy surface embedded in a non-Darcy porous medium. They examined the negative effects of the Grashof number and magnetic parameter on the local Nusselt number and the local density number of the motile microorganisms. On the other hand, the study of the entropy generation due to nanofluid flow can be found in Mansour et al. (2016), Shahi et al. (2011), Mahmoudi et al. (2013), Khorasanizadeh et al. (2013), Mehrez et al. (2013), Parvin et al. (2014), Noghrehabadi et al. (2013), Rashidi et al. (2015), Nayak et al. (2016) and Mchirgui et al. (2012). Mansour et al. (2016) reported on the entropy generation analysis in magnetohydrodynamic natural convection flow a nanofluid in a square enclosure filled with a porous medium. It is observed that the average Bejan number increases as the Hartmann number increases. Shahi et al. (2011) discussed the entropy generation due to natural convection of a Cu-water nanofluid inside an enclosure with a protruded heat source. They showed that putting the heat source mountains in the bottom wall gives the maximum values of Nusselt number and minimum entropy generation. Mahmoudi et al. (2013) focused on the entropy generation due to MHD natural convection of a water based nanofluid inside a trapezoidal enclosure. They indicated that the entropy generation is a decreasing function of a nanoparticle volume fraction, while it is increased by increasing the magnetic field parameter. The problem of heat transfer by mixed convection flow of a nanofluid in a lid-driven enclosure when the entropy generation analysis is taken into account was discussed by Khorasanizadeh et al. (2013). It is found that the minimum entropy generation occurs in pure fluid at low Rayleigh and low Reynolds numbers. In the references (Mehrez et al., 2013; Parvin et al., 2014; Noghrehabadi et al., 2013; Rashidi et al., 2015; Nayak et al., 2016) the authors focused on the entropy generation due to convective flow of nanofluids inside an open cavity, direct absorption solar collector, over a stretching sheet and past a vertical plate saturated porous medium. The entropy generation analysis due to double diffusive convection inside a square enclosure filled with porous medium using Darcy model was investigated by Mchirgui et al. (2012). The results revealed that the entropy generation decreases as the Darcy number increases. Sheikholeslami and Zeeshan (2017) discussed the Cu-water nanofluid flow in a permeable enclosure under the impact of Lorentz forces. They indicated that the heat transfer is enhanced with rise of the inclination angle and Hartmann number. The effects of thermal radiation and magnetic dipole on the ferromagnetic fluid flow over a stretching sheet were examined by Zeeshan et al. (2016).

Shehzad et al. (2016) used a Buongiorno's nanofluid model to discuss the convective heat transfer of nanofluid inside a wavy channel. Zeeshan et al. (2016) and Ellahi et al. (2016) interested with particle shape effects on the boundary layer flow of nanofluid. The results of Zeeshan and Majeed (2016) referred that the increase in the ferromagnetic interaction increases the local skin friction coefficient. Sheikholeslami and Rokni (2017) investigated the double diffusion convection in the presence of induced magnetic field using the two phase nanofluid model. Recently several authors focused on several methods of heat transfer enhancement using nanofluid (Sheikholeslami and Bhatti, 2017; Sheikholeslami and Shehzad, 2017a,b; Sheikholeslami and Sadoughi, 2017; Sheikholeslami, 2017).

Motivated by all the studies mentioned above, the main objective of this investigation is to study the entropy generation analysis due to boundary layer flow and heat transfer of a nanofluid over a vertical stretching cylinder using Buongiorno (2006) model. The novelty of the present study appears in the investigation of the case of nanofluid in which the nanoparticle volume fraction at the boundary is active control and case of the entropy generation, those are ignored by Mansour et al. (2011). In addition, common examples of the practical applications for this subject are the extrusion of metals into cooling liquids, food, plastic products, the reprocessing of material in the molten state under high temperature. The MATLAB function bvp4c is used to solve the governing equations after converting them to similar form. The viscous dissipation term in cylindrical coordinates is derived in detail and the Bejan number is defined. Far as we know, this investigation did not present before.

2. Assumption of the problem

Consider a steady two-dimensional flow of an incompressible viscous nanofluid over a vertical stretching cylinder. The physical model and coordinates system are depicted in Fig. 1. The r-axis is measured in the radial direction and the z-axis is measured along the cylinder axis. It is assumed that the flow is laminar. The model used for nanofluid includes both the Brownian motion and thermophoresis effects. Besides, the free stream conditions for temperature and nanoparticles volume fraction are T_∞ and ϕ_∞, respectively, whereas, the cylinder surface conditions for temperature are $T_w(z)$. Further, the normal fluxes of the nanoparticles volume fraction is taken to be equal zero when the thermophoresis is considered. This makes the nanoparticles volume fraction at the surface active control compared with constant conditions of the nanoparticles volume fraction. The effects of radiation, Joule heating and viscous dissipation are neglected.

3. Mathematical analysis

The first stage in our analysis is the derivation of the governing problem step by step as follows:

Introducing the governing equations in vector forms:

$$\nabla \cdot \boldsymbol{u} = 0 \tag{1}$$

$$\rho_f(\boldsymbol{u} \cdot \nabla \boldsymbol{u}) = -\nabla p + \rho^* \boldsymbol{g} + \nabla \cdot \tau \tag{2}$$

$$(\rho C)_f(\boldsymbol{u} \cdot \nabla T) = k\nabla^2 T + (\rho C)_p \left[D_B \nabla \phi \cdot \nabla T + \frac{D_T}{T_\infty} \nabla T \cdot \nabla T \right] \tag{3}$$

$$(\boldsymbol{u} \cdot \nabla \phi) = D_B \nabla^2 \phi + \frac{D_T}{T_\infty} \nabla^2 T \tag{4}$$

where $\rho^* = \phi\rho_p + (1-\phi) \times \{\rho_f(1-\beta(T-T_\infty))\}$

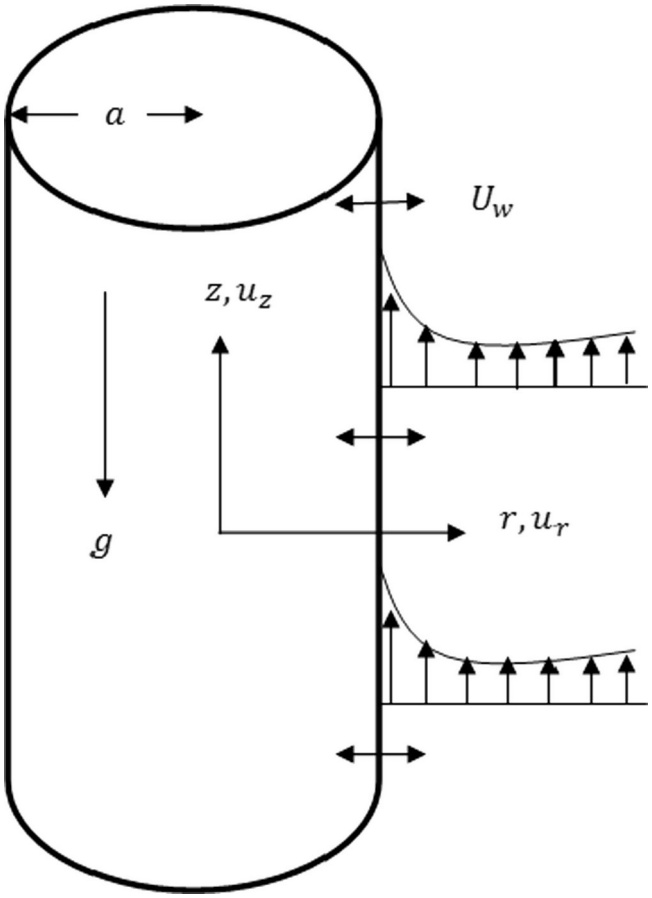

Fig. 1. Physical model and coordinate system.

In the above equations, $\boldsymbol{u} = (u_r, u_\theta, u_z)$ is the velocity vector; p is the pressure; $\boldsymbol{g}$ is the gravity acceleration vector; τ is the stress tensor; $(\rho C)_f$ is the heat capacity of the base fluid; T is the temperature; k is the thermal conductivity; $(\rho C)_p$ is the effective heat capacity of the nanoparticle material; D_B is the Brownian diffusion coefficient; ϕ is the nanoparticle volume fraction; D_T is the thermophoretic diffusion coefficient; ρ is the density and the subscripts f and p refer to the base fluid and nanoparticles, respectively.

The definition of the gradient of a scalar, the divergence of the velocity and the advection of velocity in cylindrical coordinates may be expanded, respectively, as follows:

$$\nabla\varphi = \frac{\partial\varphi}{\partial r}\hat{r} + \frac{1}{r}\frac{\partial\varphi}{\partial\theta}\hat{\theta} + \frac{\partial\varphi}{\partial z}\hat{z} \tag{5}$$

$$\nabla \cdot \boldsymbol{u} = \frac{1}{r}\frac{\partial(ru_r)}{\partial r} + \frac{1}{r}\frac{\partial u_\theta}{\partial\theta} + \frac{\partial u_z}{\partial z} \tag{6}$$

$$\boldsymbol{u} \cdot \nabla\boldsymbol{u} = \begin{cases} u_r\frac{\partial u_r}{\partial r} + \frac{u_\theta}{r}\frac{\partial u_r}{\partial\theta} - \frac{u_\theta^2}{r} + u_z\frac{\partial u_r}{\partial z} \\ u_r\frac{\partial u_\theta}{\partial r} + \frac{u_\theta}{r}\frac{\partial u_\theta}{\partial\theta} + \frac{u_r u_\theta}{r} + u_z\frac{\partial u_\theta}{\partial z} \\ u_r\frac{\partial u_z}{\partial r} + \frac{u_\theta}{r}\frac{\partial u_z}{\partial\theta} + u_z\frac{\partial u_z}{\partial z} \end{cases} \tag{7}$$

Also, taking into account the advantage of the symmetry of the stress tensor, the divergence of stress tensor in the cylindrical coordinates is presented as:

$$\nabla \cdot \tau = \begin{cases} \frac{1}{r}\frac{\partial(r\tau_{rr})}{\partial r} + \frac{1}{r}\frac{\partial(\tau_{r\theta})}{\partial\theta} - \frac{\tau_{\theta\theta}}{r} + \frac{\partial(\tau_{rz})}{\partial z} \\ \frac{1}{r}\frac{\partial(\tau_{\theta\theta})}{\partial\theta} + \frac{\partial(\tau_{r\theta})}{\partial r} + \frac{2\tau_{r\theta}}{r} + \frac{\partial(\tau_{\theta z})}{\partial z} \\ \frac{1}{r}\frac{\partial(r\tau_{rz})}{\partial r} + \frac{1}{r}\frac{\partial(\tau_{\theta z})}{\partial\theta} + \frac{\partial(\tau_{zz})}{\partial z} \end{cases} \tag{8}$$

where the components of the stress tensor in cylindrical coordinates are expressed as:

$$\tau_{rr}=2\mu_f\frac{\partial u_r}{\partial r},\ \ \tau_{\theta\theta}=2\mu_f\left[\frac{1}{r}\frac{\partial(u_\theta)}{\partial\theta}+\frac{u_r}{r}\right],\ \ \tau_{zz}=2\mu_f\frac{\partial u_z}{\partial z},$$
$$\tau_{r\theta}=\mu_f\left[r\frac{\partial}{\partial r}\left(\frac{u_\theta}{r}\right)+\frac{1}{r}\frac{\partial u_r}{\partial\theta}\right],\ \ \tau_{\theta z}=\mu_f\left[\frac{\partial(u_\theta)}{\partial z}+\frac{1}{r}\frac{\partial u_z}{\partial\theta}\right],$$
$$\tau_{rz}=\mu_f\left[\frac{\partial(u_z)}{\partial r}+\frac{\partial u_r}{\partial z}\right] \tag{9}$$

For a two-dimensional flow and using Eqs. (5)–(9) and considering the boundary layer approximations, the governing equations of the problem are written as:

$$\frac{\partial u_r}{\partial r}+\frac{\partial u_z}{\partial z}+\frac{u_r}{r}=0 \tag{10}$$

$$\rho_f\left[u_z\frac{\partial u_z}{\partial z}+u_r\frac{\partial u_z}{\partial r}\right]=\mu_f\left[\frac{\partial^2u_z}{\partial r^2}+\frac{1}{r}\frac{\partial u_z}{\partial r}\right]+((1-\phi_\infty)\rho_{f\infty}\beta g(T-T_\infty)-(\rho_p-\rho_{f\infty})(\phi-\phi_\infty)g) \tag{11}$$

$$\rho_f\left[u_z\frac{\partial u_r}{\partial z}+u_r\frac{\partial u_r}{\partial r}\right]=-\frac{\partial p}{\partial r}+\mu_f\left[\frac{\partial^2u_r}{\partial r^2}+\frac{1}{r}\frac{\partial u_r}{\partial r}-\frac{u_r}{r^2}\right] \tag{12}$$

$$(\rho C)_f\left[u_z\frac{\partial T}{\partial z}+u_r\frac{\partial T}{\partial r}\right]=k\left[\frac{\partial^2T}{\partial r^2}+\frac{1}{r}\frac{\partial T}{\partial r}\right]+(\rho C)_p\left\{D_B\left(\frac{\partial T}{\partial r}\cdot\frac{\partial\phi}{\partial r}\right)+\frac{D_T}{T_\infty}\left(\frac{\partial T}{\partial r}\right)^2\right\} \tag{13}$$

$$u_z\frac{\partial\phi}{\partial z}+u_r\frac{\partial\phi}{\partial r}=D_B\left[\frac{\partial^2\phi}{\partial r^2}+\frac{1}{r}\frac{\partial\phi}{\partial r}\right]+\frac{D_T}{T_\infty}\left[\frac{\partial^2T}{\partial r^2}+\frac{1}{r}\frac{\partial T}{\partial r}\right] \tag{14}$$

The boundary conditions are expressed as:

$$r=a,\ \ u_r=U_w,\ \ u_z=V_w,\ \ T=T_w(z)=T_\infty(z)+Az^n,\ \ D_B\frac{\partial\phi}{\partial r}+\frac{D_T}{T_\infty}\frac{\partial T}{\partial r}=0, \tag{15a}$$

$$r\to\infty,\ \ u_z\to0,\ \ T\to T_\infty(z),\ \ \phi\to\phi_\infty(z) \tag{15b}$$

where $U_w=-ca\gamma,\ \ V_w=2cz,\ \ c$ is a positive constant and γ is a constant such that $\gamma>0$ refers to mass suction and $\gamma<0$ refers to mass injection. Also, $T_\infty(z)$ and $\phi_\infty(z)$ are considered to be equal $T_0+\frac{n}{1-n}Az^n$ and $\phi_0+\frac{n}{1-n}Az^n$, respectively, with a reference temperature $T_0(0)$ and a reference nanoparticle volume fraction $\phi_0(0)$. Further n is the thermal stratification parameter with the range $0\leqslant n\leqslant1$ and the suffices w and ∞ denote surface and ambient conditions.

Introducing the following similarity transformations, see Wang (1988):

$$\eta=\left(\frac{r}{a}\right)^2,\ \ u_r=-ca\frac{F(\eta)}{\sqrt{\eta}},\ \ u_z=2czF'(\eta),\ \ \vartheta=\frac{T-T_\infty}{T_w-T_\infty},\ \ S=\frac{\phi-\phi_\infty}{\phi_w-\phi_\infty} \tag{16}$$

Substituting Eq. (16) in Eqs. (11), (13) and (14), the following ordinary differential equations are obtained:

$$\eta F'''+F''+Re[FF''-F'^2+Gr[\vartheta-NrS]]=0 \tag{17}$$

$$\eta\vartheta''+(1+RePrf)\vartheta'-nRePrf'\left[\vartheta+\frac{n}{1-n}\right]+Pr\eta(N_bS'\vartheta'+N_t\vartheta'^2)=0 \tag{18}$$

$$\eta S''+(1+ReLef)S'-nReLef'\left[S+\frac{n}{1-n}\right]+\frac{N_t}{N_b}(\eta\vartheta''+\vartheta')=0 \tag{19}$$

where the prime denotes the differentiation with respect to η and $Re=\frac{ca^2}{2\upsilon_f}$ is the Reynolds number, $Pr=\frac{\upsilon_f}{\alpha}$ is the Prandtl number, $Le=\frac{\upsilon_f}{D_B}$ is the Lewis number, $N_b=\frac{(\rho C)_pD_B(\phi_w-\phi_\infty)}{\upsilon_f(\rho C)_f}$ is the Brownian motion parameter, $N_t=\frac{(\rho C)_pD_T(T_w-T_\infty)}{T_\infty\upsilon_f(\rho C)_f}$ is the thermophoresis parameter, $Nr=\frac{(\rho_p-\rho_{f\infty})(\phi-\phi_\infty)}{(1-\phi_\infty)\rho_{f\infty}\beta(T_w-T_\infty)}$ is the buoyancy ratio, $Gr=\frac{(1-\phi_\infty)\rho_{f\infty}\beta g(T_w-T_\infty)}{\rho_f4c^2z}=\frac{(1-\phi_\infty)\rho_{f\infty}\beta g(T_w-T_\infty)z}{\rho_fV_w^2}$ is the Grashof number.The boundary conditions are, also, converted to:

$$F=\gamma,\ \ F'=1,\ \ \vartheta=1,\ \ N_bS'+N_t\vartheta'=0at\eta=1. \tag{20a}$$

$$F'\to0,\ \ \vartheta\to0,\ \ S\to0\ \ \text{as}\ \ \eta\to\infty. \tag{20b}$$

As it has been referred by Kuznetsov and Nield (2013), the local Sherwood number, in this case is identically zero; however, the local skin-friction coefficient and the local Nusselt number are, respectively, given by:

$$C_f=\frac{2\mu_f}{\rho_fV_w^2}\left[\frac{\partial u_z}{\partial r}\right]_{r=a} \tag{21}$$

$$Nu=\frac{-a}{\Delta T}\left[\frac{\partial T}{\partial r}\right]_{r=a} \tag{22}$$

Using the dimensionless quantities presented in Eq. (16), Eqs. (21) and (22) are converted to:

$$\frac{Rez}{a}C_f=F''(1) \tag{23}$$

$$Nu=-2\vartheta'(1) \tag{24}$$

4. Entropy generation analysis

In the present problem, the entropy generation consists of three sources. i.e. entropy generation due to heat transfer, viscous dissipation and mass diffusion, as presented in Mchirgui et al. (2012). Here, the equation of the entropy is expressed as:

$$S_G=\frac{k}{T_\infty^2}(\nabla T)^2+\frac{\mu_f}{T_\infty}\Phi+\frac{RdD_B}{\phi_\infty}(\nabla\phi)^2+\frac{RdD_B}{T_\infty}\nabla\phi\cdot\nabla T \tag{25}$$

At this point, it is important to derive the form of viscous dissipation term in cylindrical coordinates as follows:

$$\Phi=\frac{1}{\mu_f}\tau:\nabla\boldsymbol{u} \tag{26}$$

Using Eqs. (8) and (9), Eq. (26) can be written as:

$$\Phi=2\left[\frac{\partial u_r}{\partial r}\right]^2+2\left[\frac{1}{r}\frac{\partial u_\theta}{\partial\theta}+\frac{u_r}{r}\right]^2+2\left[\frac{\partial u_z}{\partial z}\right]^2+\left[r\frac{\partial(u_\theta/r)}{\partial r}+\frac{1}{r}\frac{\partial u_r}{\partial\theta}\right]^2+\left[\frac{1}{r}\frac{\partial u_z}{\partial\theta}+\frac{\partial u_\theta}{\partial z}\right]^2+\left[\frac{\partial u_z}{\partial r}+\frac{\partial u_r}{\partial z}\right]^2 \tag{27}$$

For two dimensional flow and using Eq. (5), the entropy equation is given by:

$$S'''=\frac{k}{T_\infty^2}\left[\left(\frac{\partial T}{\partial r}\right)^2+\left(\frac{\partial T}{\partial z}\right)^2\right]+\frac{RdD_B}{\phi_\infty}\left[\left(\frac{\partial\phi}{\partial r}\right)^2+\left(\frac{\partial\phi}{\partial z}\right)^2\right]+\frac{RdD_B}{T_\infty}\left[\frac{\partial T}{\partial r}\frac{\partial\phi}{\partial r}+\frac{\partial T}{\partial z}\frac{\partial\phi}{\partial z}\right]+\frac{\mu_f}{T_\infty}\left[2\left[\frac{\partial u_r}{\partial r}\right]^2+2\left[\frac{\partial u_z}{\partial z}\right]^2+\left[\frac{\partial u_z}{\partial r}+\frac{\partial u_r}{\partial z}\right]^2\right] \tag{28}$$

Using boundary layer approximations:

$$S''' = \frac{k}{T_\infty^2}\left[\left(\frac{\partial T}{\partial r}\right)^2\right] + \frac{RdD_B}{\phi_\infty}\left[\left(\frac{\partial \phi}{\partial r}\right)^2\right] + \frac{RdD_B}{T_\infty}\left[\frac{\partial T}{\partial r}\frac{\partial \phi}{\partial r}\right] + \frac{\mu_f}{T_\infty}\left(\frac{\partial u}{\partial r}\right)^2 \tag{29}$$

Converting Eq. (29) to dimensionless form using characteristic entropy generation rate S_0''' as:

$$NS = \frac{S'''}{S_0'''} \tag{30}$$

where;

$$S_0''' = \frac{k(\Delta T)^2}{(aT_\infty)^2} \tag{31}$$

Using Eq. (16), the similar form of Eq. (30) is obtained as follows:

$$NS = S_T + S_\phi + S_F \tag{32}$$

where $S_T = 4\eta\vartheta'^2$, $S_\phi = \epsilon\left[\frac{\Sigma}{\Omega}\right]^2(4\eta\phi'^2) + \epsilon\frac{\Sigma}{\Omega}(4\eta\phi'\vartheta')$, $S_F = \frac{Br}{\Omega}\left[\frac{F}{2\eta} - F'\right]^2$In Eq. (32), $\Omega = \frac{\Delta T}{T_\infty}$ is the dimensionless temperature difference, $\Sigma = \frac{\Delta\phi}{\phi_\infty}$ is the dimensionless concentration difference, $Br = \frac{\mu_f V_w^2}{k\Delta T}$ is the Brinkman number and $\epsilon = \frac{RdD_B\phi_\infty}{k}$ is dimensionless constant. Also, S_T is the dimensionless entropy generation due to the heat transfer irreversibility, S_ϕ is the entropy generation due to mass diffusion and S_F is the entropy generation due to viscous dissipation.

The Bejan number *Be* is defined as the ratio between the entropy generations due to heat transfer S_T and the total entropy generation *NS* and it can be written as:

$$Be = \frac{S_T}{NS} \tag{33}$$

5. Numerical section and validation

Numerical method used to solve the equations (17)–(19) depends, strongly, on the MATLAB software. Here, we need to reduce the higher order derivatives with respect to η. This can be obtained by introducing the following new variables:

$$F = Y_1(\eta),\ F' = Y_2(\eta),\ F'' = Y_3(\eta),\ \vartheta = Y_4(\eta),\ \vartheta' = Y_5(\eta),$$
$$S = Y_6(\eta),\ S' = Y_7(\eta) \tag{34}$$

Using (34), Eqs. (17)–(19) transform to the following first order differential system:

$$\frac{dY_1}{d\eta} = Y_2 \tag{35a}$$

$$\frac{dY_2}{d\eta} = Y_3 \tag{35b}$$

$$\frac{dY_3}{d\eta} = \frac{(-Y_3 - Re[Y_1Y_3 - Y_2^2 + Gr[Y_4 - NrY_6]])}{\eta} \tag{35c}$$

$$\frac{dY_4}{d\eta} = Y_5 \tag{35d}$$

$$\frac{dY_5}{d\eta} = \frac{\left(-(1 + RePrY_1)Y_5 + nRePrY_2\left[Y_4 + \frac{n}{1-n}\right] - Pr\eta(N_bY_5Y_7 + N_tY_5^2)\right)}{\eta} \tag{35e}$$

$$\frac{dY_6}{d\eta} = Y_7 \tag{35f}$$

$$\frac{dY_7}{d\eta} = \frac{\left(-(1 + ReLeY_1)Y_7 + nReLeY_2\left[Y_6 + \frac{n}{1-n}\right] + \frac{N_t}{N_b}(\eta\frac{dY_5}{d\eta} + Y_5)\right)}{\eta} \tag{35g}$$

Subject to the following boundary conditions:

$$Y_1(1) = \gamma,\ Y_2(1) = 1,\ Y_4(1) = 1,\ N_bY_7(1) + N_tY_5(1) = 0 \tag{36a}$$

$$Y_2(\eta_{max}) = 0,\ Y_4(\eta_{max}) = 0,\ Y_6(\eta_{max}) = 0 \tag{36b}$$

The second step in this technique is calling the function *bvp4c* from MATLAB library to solve the previous system. The value of η_{max} is 20, while the step size is 0.04. Also, the accuracy of this method is tested by comparing the obtained data with those obtained by Mansour et al. (2011), Wang (1988) and Ishak et al. (2008). Fig. 2 shows excellent agreements are found between the present results and previously published results.

6. Results and discussion

The obtained numerical results are discussed in this section. The governing physical parameters are Grashof number *Gr*, suction/injection parameter γ, the index parameter *n*, the Reynolds number *Re*, the thermophysical parameter N_t, the Brownian motion parameter N_b and the buoyancy parameter *Nr* those are varied in wide ranges i.e. $0 \leqslant Gr \leqslant 5$, $-0.5 \leqslant \gamma \leqslant 0.5$, $0 \leqslant n \leqslant 0.5$, $0.5 \leqslant Re \leqslant 3$, $0.1 \leqslant N_t \leqslant 0.5$, $0.1 \leqslant N_b \leqslant 0.5$, $0.1 \leqslant Nr \leqslant 0.5$, respectively. For the nanofluid model, water is considered as a base fluid with $Pr = 7.0$. The data is depicted in Figs. 2–14 in terms of velocity profiles, temperature distributions, nanoparticle volume fraction profiles and local entropy generation rate. The values of skin friction coefficient and local Nusselt number are presented in Tables 1–3. The values of $\epsilon = 0.001$, $\Sigma = 0.01$, $\Omega = 100$ and $Br = 1$ are taken into account through the procedures.

Figs. 3–6 show the profiles of velocity, temperature, nanoparticles volume fraction and entropy generation for different values of Grashof number *Gr*. Here, three values of suction/injection parameter γ are considered. The value of $\gamma = -0.5$ represents the injection case, the value of $\gamma = 0$ denotes the impermeable cylinder and the value of $\gamma = 0.5$ refers to the suction case. The results reveal that the increase in *Gr* enhances the nanofluid velocity, nanoparticle volume fraction distributions and local entropy generation rate, while on contrary, the temperature distributions are

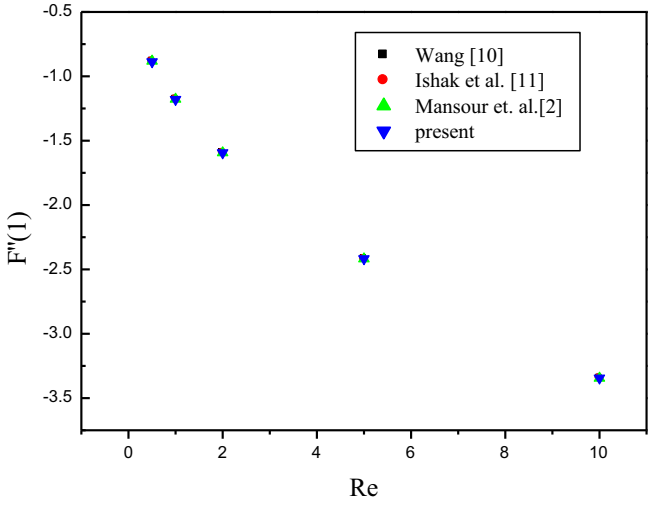

Fig. 2. Validation test at $Gr = 0$ and $\gamma = 0$.

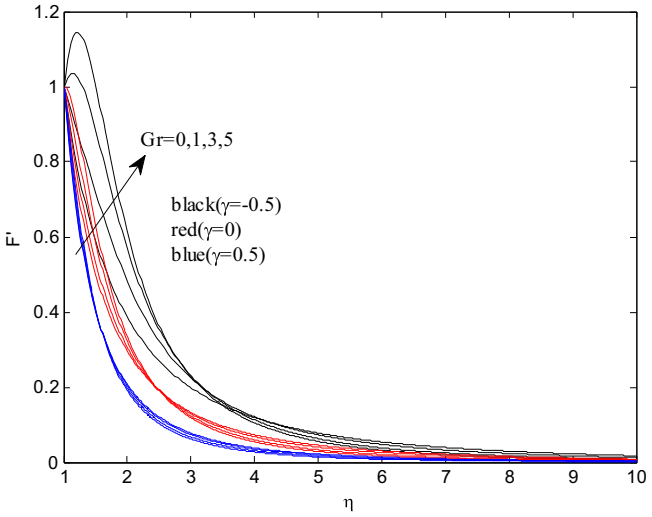

Fig. 3. Profiles of the dimensionless velocity for different values of Gr and γ at $Re = 2,\ Nr = N_b = N_t = 0.1,\ n = 0.1,\ Pr = 7.0,\ Le = 2$.

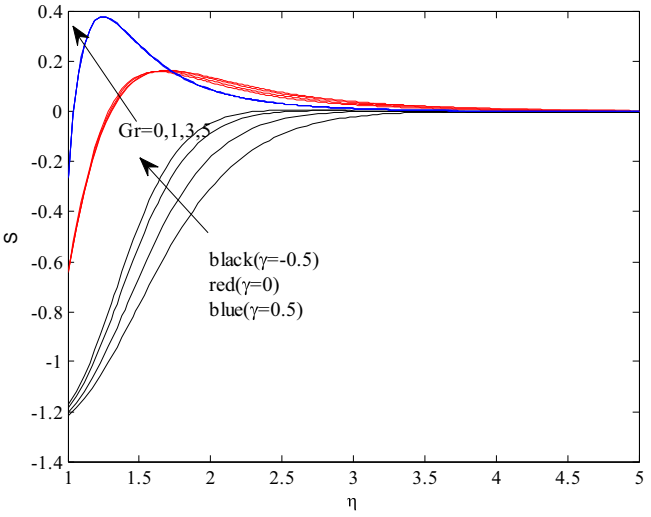

Fig. 5. Profiles of the nanoparticle volume fraction for different values of Gr and γ at $Re = 2,\ Nr = N_b = N_t = 0.1,\ n = 0.1,\ Pr = 0.7,\ Le = 2$.

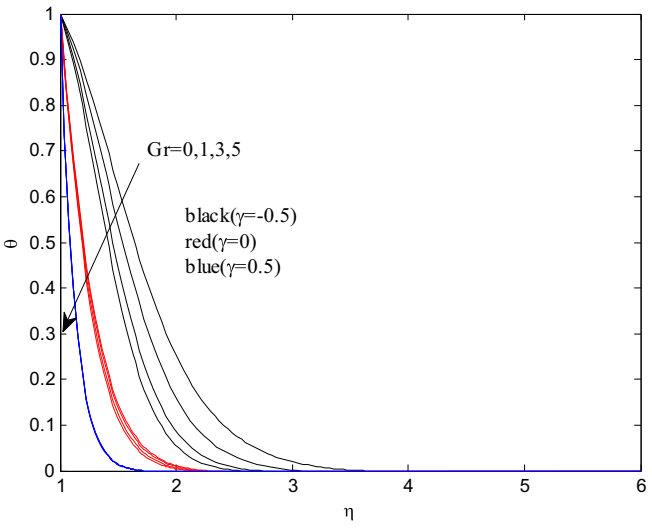

Fig. 4. Profiles of the dimensionless temperature for different values of Gr and γ at $Re = 2,\ Nr = N_b = N_t = 0.1,\ n = 0.1,\ Pr = 7.0,\ Le = 2$.

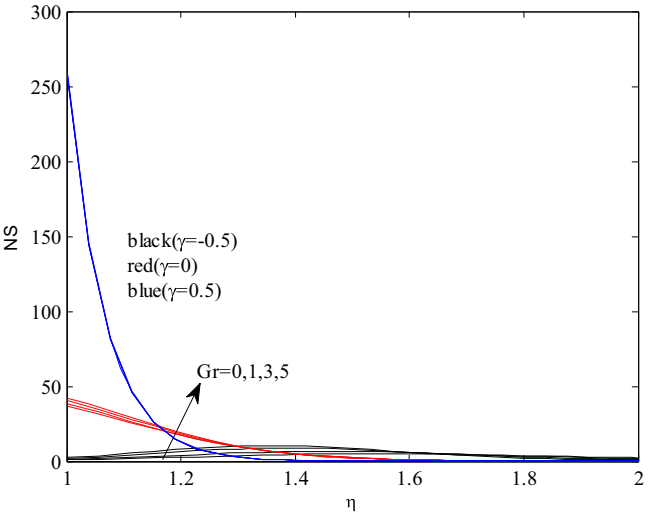

Fig. 6. Profiles of the entropy generation for different values of Gr and γ at $Re = 2,\ Nr = N_b = N_t = 0.1,\ n = 0.1,\ Pr = 7.0,\ Le = 2$.

reduced by increase Gr. The physical explanation of these behaviors is due to the buoyancy force arising from the temperature difference inside the flow domain. This force makes the fluid flows rapidly. Beside, based on the fact that the increase in the velocity decreases the temperature, the effect of Gr on the temperature distributions can be explained. Further, the increase in suction/injection parameter causes a decrease in the velocity profiles and temperature distributions, while it increases the distributions of nanoparticle volume fraction. This can be attributed to the total mass of the nanofluid that decreases in the suction case ($\gamma > 0$) which makes the fluid movement slower. Also, the suction case makes the fluid cooler and hence the temperature distributions decreases. In addition, Fig. 6 shows that the entropy generation takes its maximum values in the suction case and takes its minimum values in the injection case. This behavior is due to the momentum boundary layer thickness and thermal boundary layer thickness those have a dominance effect on the entropy generation in the suction case.

Figs. 7–10 display the profiles of velocity, temperature, nanoparticles volume fraction and local entropy generation for different values of Reynolds number Re and thermal stratification parameter n. It should be mentioned that the case of $n = 0$ means the temperature difference in the flow domain is constant and $n = 0.5$ means variable temperature differences. It is clear that the increase in Re acts as a retarding force for the nanofluid flow. Like the velocity behavior, the temperature distributions decrease as Re increases, while on contrary, the nanoparticle volume fraction and the local entropy generation get higher values by increase Re. Moreover, the thermal stratification effect gives behavior similar to the effect of Re on F′, ϑ, S. However, the local entropy generation is very sensitive for the increase in thermal stratification parameter. The increase in n enhances the temperature gradients in the flow region. Consequently, the local entropy generation increases, slightly, by increasing n. To explain the thermal stratification effect, it should be referred to its definition. When the nanofluid is warmer than 4 °C it gets less dense for each increment in degree Celsius. This allows for thermal layering; where warmer nanofluid is stored on top of colder nanofluid this phenomenon defined as "thermal stratification". Now, the increase in n leads to decrease the temperature difference which in turn decreases the mixed convection.

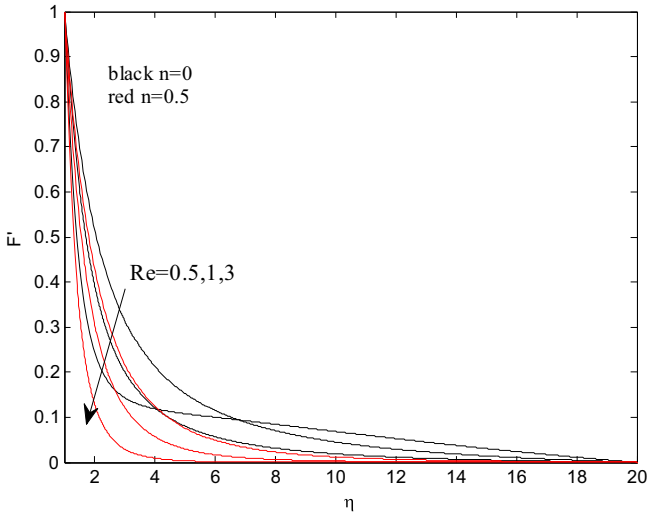

Fig. 7. Profiles of the dimensionless velocity for different values of *Re* and *n* at $Gr = 1,\ Nr = N_b = N_t = 0.1,\ \gamma = 0.2,\ Pr = 7.0,\ Le = 2$.

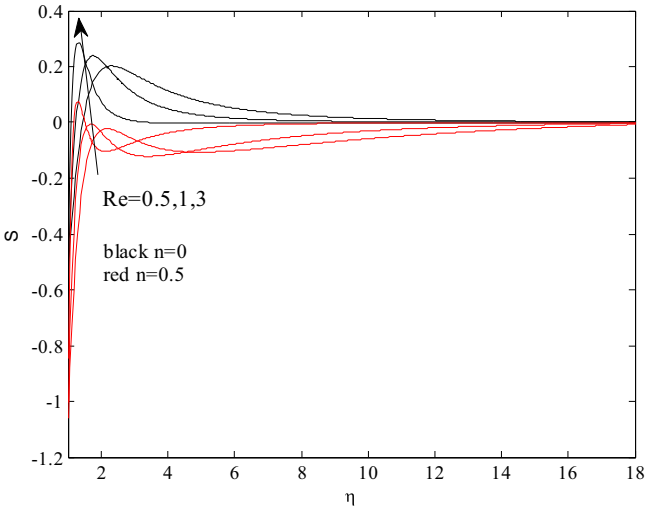

Fig. 9. Profiles of the nanoparticle volume fraction for different values of *Re* and *n* at $Gr = 1,\ Nr = N_b = N_t = 0.1,\ \gamma = 0.2,\ Pr = 7.0,\ Le = 2$.

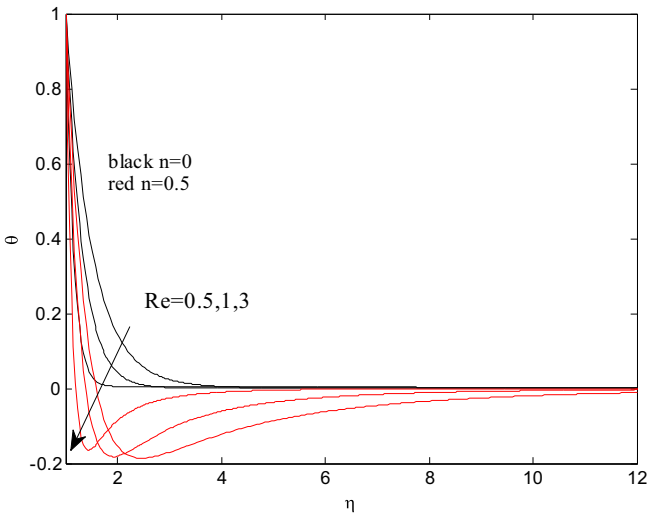

Fig. 8. Profiles of the dimensionless temperature for different values of *Re* and *n* at $Gr = 1,\ Nr = N_b = N_t = 0.1,\ \gamma = 0.2,\ Pr = 7.0,\ Le = 2$.

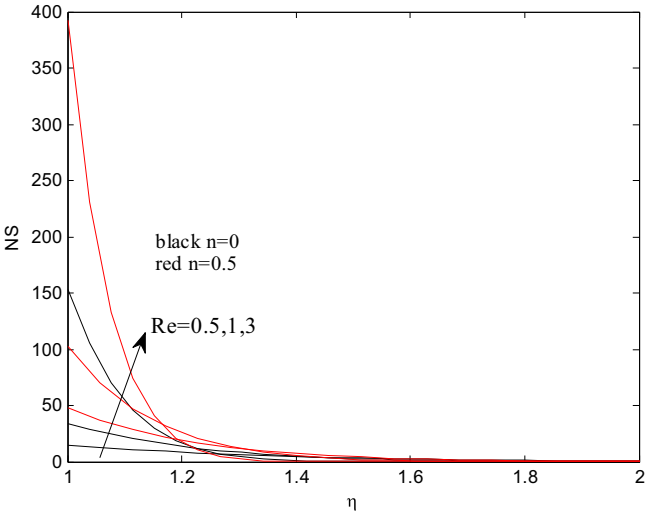

Fig. 10. Profiles of the entropy generation for different values of *Re* and *n* at $Gr = 1,\ Nr = N_b = N_t = 0.1,\ \gamma = 0.2,\ Pr = 7.0,\ Le = 2$.

In Fig. 11, the profiles of the dimensionless velocity for different values of thermophysics parameter are plotted. It is observed that the velocity profiles are reduced by the increase in *Nt*. Besides, Fig. 12 is plotted to visualize the distributions of nanoparticle volume fraction for different values of Nt. Here, the negative values of nanoparticle volume fraction is due to the fact that the effect of thermophoresis is such that an elevation. Hence, there exists a depression in the relative value of nanoparticle volume fraction at the wall (see Kuznetsov and Nield, 2013). Moreover, the increase in *Nt* causes a clear enhancement in the distributions of $S(\eta)$, particularly, near the wall. Fig. 13 shows the temperature distributions for different values of Nt. The results indicated that the increase in Nt enhances the temperature distributions and this is due to the buoyancy force resulting from the temperature difference $(T_w - T_\infty)$ inside the flow domain. Unlike the effect of Nt on $S(\eta)$, the increase in *Nb* leads to vanishing the behavior of S, as it can be noted in Fig. 14. The velocity profiles and temperature distributions are insensitive with the variations of *Nb* and thus it is omitted. In Fig. 15, the influence of buoyancy ratio on the velocity profiles is depicted. The increase in Nr declares the nanofluid motion. This can be attributed to the temperature differences inside the boundary layer that decreases by the increase in Nr and as a result the mixed convection decreases.

Lastly, Tables 1–3 present the values of skin friction coefficient $F''(1)$ and local Nusselt number $-2\vartheta'(1)$ for different values of *Gr*, γ, Re, *n*, Nr and *Nb*. The results indicated that all the values of $F''(1)$ is negative in the case of $\gamma > 0$ (suction case). In addition, the increase in γ leads to increase the momentum and thermal boundary layer thickness. Therefore, the absolute values of $F''(1)$ and the rate of heat transfer $-2\vartheta'(1)$ increase as γ increases. Besides, the increase in Gr causes enhancement in the local Nusselt number, whereas it decreases $|F''(1)|$. Further, both of $|F''(1)|$ and $-2\vartheta'(1)$ increase as the thermal stratification parameter *n* or Reynolds number *Re* increases. The effect of Nr on $|F''(1)|$ is more significant at the low values of Nb (Nb = 0.1) compared with the case of Nb = 0.3. morevere, $|F''(1)|$ increases as Nr increases. This behavior is observed for Nb = 0.1, while on contrary the case Nb = 0.3, $|F''(1)|$ is reduced as Nr increases. The local Nusselt decreases as Nr increases for all values of Nb. In addition, the increase in *Nb* enhances the rate of heat transfer.

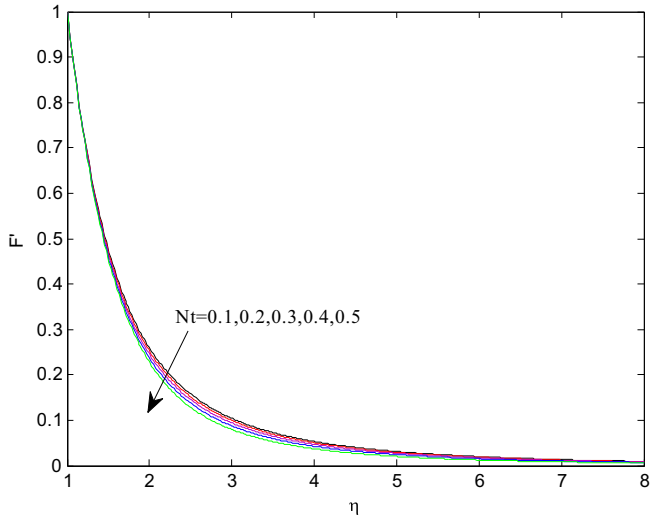

Fig. 11. Profiles of the dimensionless velocity for different values of Nt at $Re = 2,\ n = 0.1,\ Gr = 1,\ Nr = N_b = N_t = 0.1,\ \gamma = 0.2,\ Pr = 7.0,\ Le = 2$.

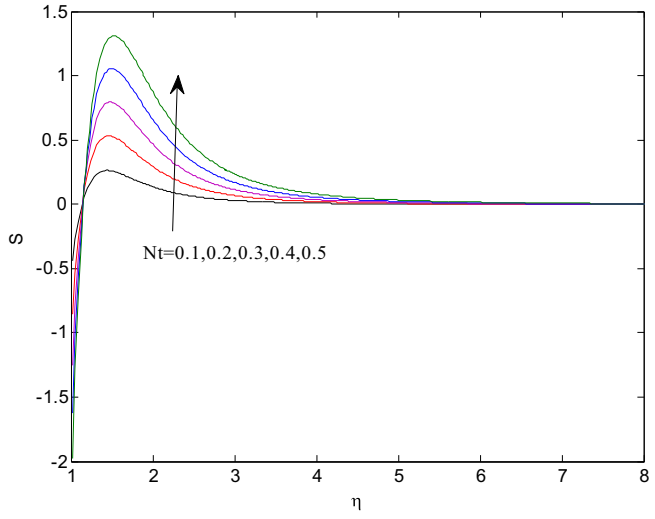

Fig. 12. Profiles of the nanoparticle volume fraction for different values of Nt at $Re = 2,\ n = 0.1,\ Gr = 1,\ Nr = N_b = N_t = 0.1,\ \gamma = 0.2,\ Pr = 7.0,\ Le = 2$.

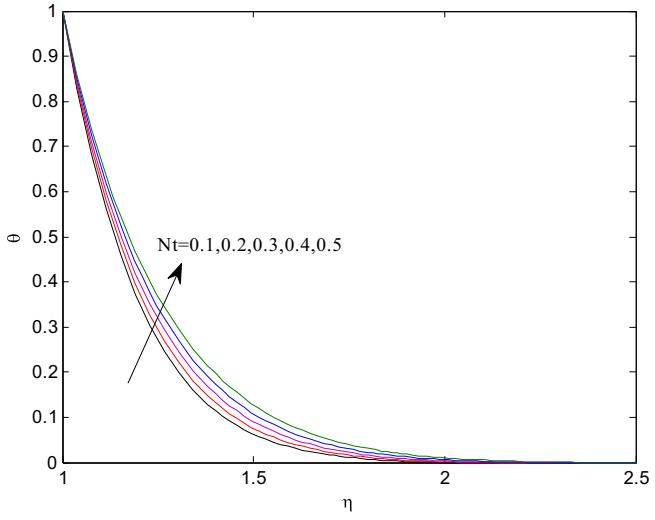

Fig. 13. Profiles of dimensionless temperature for different values of Nt at $Re = 2,\ n = 0.1,\ Gr = 1,\ Nr = N_b = 0,\ \gamma = 0.2,\ Pr = 7.0,\ Le = 2$.

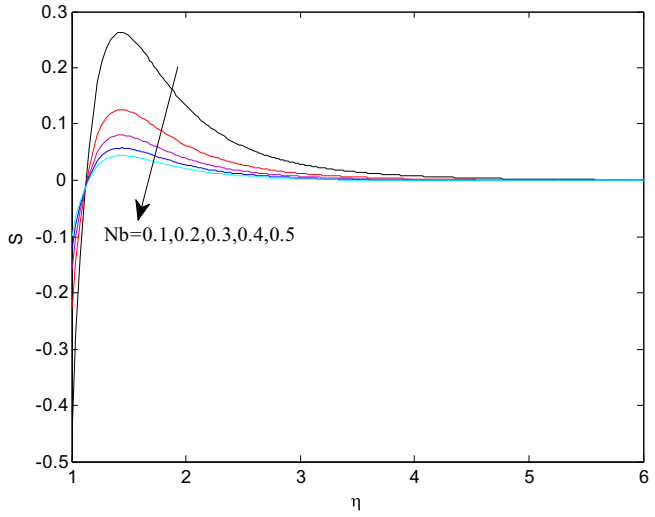

Fig. 14. Profiles of the nanoparticle volume fraction for different values of Nb at $Re = 2,\ n = 0.1,\ Gr = 1,\ Nr = N_t = 0.1,\ \gamma = 0.2,\ Pr = 7.0,\ Le = 2$.

Table 1
Values of skin-friction coefficient and local Nusselt number for different values of Gr and γ at $Re = 2, Nr = N_b = N_t = 0.1, n = 0.1, Pr = 0.7, Le = 2$.

γ	Gr	$F''(1)$	$-2\vartheta'(1)$
−0.5	0	−1.1812	0.9495
	1	−0.5315	1.1241
	3	0.5513	1.3530
	5	1.5029	1.5229
0	0	−1.5944	6.0671
	1	−1.2353	6.1687
	3	−0.5520	6.3461
	5	0.0956	6.4990
0.5	0	−2.1472	16.0439
	1	−1.9732	16.0604
	3	−1.6258	16.0938
	5	−1.2793	16.1274

Table 2
Values of skin-friction coefficient and local Nusselt number for different values of Re and n at $Gr = 1,\ Nr = N_b = N_t = 0.1,\ \gamma = 0.2,\ Pr = 0.7,\ Le = 2$.

n	Re	$F''(1)$	$-2\vartheta'(1)$
0	0.1	−0.4231	1.6599
	0.5	−0.7635	3.8315
	1	−1.0578	5.8323
	3	−1.8212	12.3603
0.5	0.1	−0.4950	3.0380
	0.5	−0.9272	6.8962
	1	−1.2657	10.1446
	3	−2.1996	19.8017

Table 3
Values of skin-friction coefficient and local Nusselt number for different values of Nb and Nr at $Re = 2,\ Gr = 1,\ N_t = 0.1,\ \gamma = 0.2,\ n = 0.1,\ Pr = 0.7,\ Le = 2$.

Nb	Nr	$F''(1)$	$-2\vartheta'(1)$
0.1	0	−1.5167	9.7463
	0.1	−1.5330	9.7358
	0.3	−1.5684	9.7128
0.3	0	−1.5169	9.7551
	0.1	−1.5212	9.7523
	0.3	−1.5299	9.7466

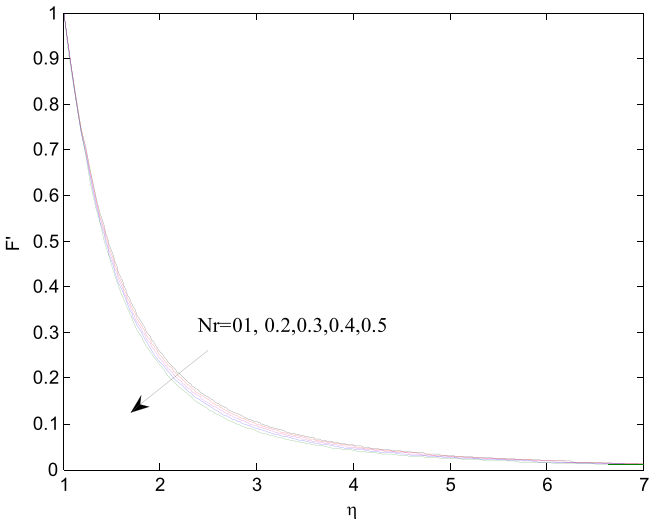

Fig. 15. Profiles of the dimensionless velocity for different values of Nr at $Re = 2,\ n = 0.1,\ Gr = 1,\ Nr = Nb = N_t = 0.1,\ \gamma = 0.2,\ Pr = 7.0,\ Le = 2$.

7. Conclusions

The steady two-dimensional boundary layer flow and heat transfer of nanofluids over a vertical permeable stretching cylinder in the presence of thermal stratification effect was, theoretically, studied. The entropy generation analysis due to this type of convective heat transfer was employed. A comprehensive analysis for the governing equations including the derivation of these equations in cylindrical coordinates, similar solutions and numerical method was presented. Comparisons with previously published results were produced and found to be in excellent agreements. From the present study, the following findings are concluded:

- The maximum values of the entropy generation occur in the suction case, while on contrary the injection case minimizes the entropy generation.
- The increase in the thermal stratification parameter enhances the entropy generation.
- The increase in the Grashof number increases the velocity profiles and nanoparticle volume fraction, whereas it reduces the temperature distributions.
- The increase in the suction/injection parameter or Reynolds number causes a reduction in profiles of the velocity and temperature; however, it increases the nanoparticle volume fraction.
- The thermal stratification parameter has negative effect on the profiles of velocity, temperature and nanoparticle volume fraction.
- The increase in the thermophoresis parameter reduces the velocity profiles, while it enhances both the temperature and nanoparticle volume fraction distributions.
- The Brownian motion parameter has negative effect on the nanoparticle volume fraction distributions, while the velocity and temperature is insensitive with the variation of the Brownian motion parameter.
- The increase in the buoyancy ratio impedes the fluid flow.

Acknowledgements

The authors would like to express their gratitude to King Khalid University, Saudia Arabia for providing administrative and technical support.

References

Ahmed, S.E., Mahdy, A., 2016. Laminar MHD natural convection of nanofluid containing gyrotactic microorganisms over vertical wavy surface saturated non-Darcian porous media. Appl. Math. Mech.-Eng. Ed. http://dx.doi.org/10.1007/s10483-016-0-9.

Ahmed, S.E., Hussein, A.K., Mohammed, H.A., Sivasankaran, S., 2014. Boundary layer flow and heat transfer due to permeable stretching tube in the presence of heat source/sink utilizing nanofluids. Appl. Math. Comput. 238, 149–162.

Anwar, I., Amin, N., Pop, I., 2008. Mixed convection boundary layer flow of a viscoelastic fluid over a horizontal circular cylinder. Int. J. Non-Linear Mech. 43, 814–821.

Bachok, N., Ishak, A., 2010. Flow and heat transfer over a stretching cylinder with prescribed surface heat flux. Malaysian J. Math. Sci. 4 (2), 159–169.

Buongiorno, J., 2006. Convective transport in nanofluids. ASME J. Heat Transfer 128, 240–250.

Ellahi, R., Zeeshan, A., Hassan, M., 2016. Particle shape effects on Marangoni convection boundary layer flow of a nanofluid.“. Int. J. Numer. Methods Heat Fluid Flow 26 (7), 2160–2174.

Elshehabey, H.M., Ahmed, S.E., 2015. MHD mixed convection in a lid-driven filled by a nanofluid with sinusoidal temperature distribution on the both vertical walls using Buongiorno’s nanofluid model. Int. J. Heat Mass Transfer 88, 181–202.

Grosan, T., Pop, I., 2011. Axisymmetric mixed convection boundary layer flow past a vertical cylinder in a nanofluid. Int. J. Heat Mass Transfer 54, 3139–3145.

Ishak, A., Nazar, R., Pop, I., 2008. Uniform suction/blowing effect on flow and heat transfer due to a stretching cylinder. Appl. Math. Modell. 32, 2059–2066.

Kakaç, S., Pramuanjaroenkij, A., 2009. Review of convective heat transfer enhancement with nanofluids. Int. J. Heat Mass Transfer 52, 3187–3196.

Khan, W., Pop, I., 2010. Boundary-layer flow of a nanofluid past a stretching sheet. Int. J. Heat Mass Transfer 53, 2477–2483.

Khorasanizadeh, H., Nikfar, M., Amani, J., 2013. Entropy generation of Cu–water nanofluid mixed convection in a cavity. Eur. J. Mech. B/Fluids 37, 143–152.

Kuznetsov, A.V., Nield, D.A., 2010. Natural convective boundary-layer flow of a nanofluid past a vertical plate. Int. J. Therm. Sci. 49, 243–247.

Kuznetsov, A.V., Nield, D.A., 2013. The Cheng-Minkowycz problem for natural convective boundary layer flow in a porous medium saturated by a nanofluid: a revised model. Int. J. Heat Mass Transfer 65, 682–685.

Kuznetsov, A.V., Nield, D.A., 2014. Natural convective boundary-layer flow of a nanofluid past a vertical plate: a revised model. Int. J. Therm. Sci. 77, 126–129.

Mahmoudi, A.H., Pop, I., Shahi, M., Talebi, F., 2013. MHD natural convection and entropy generation in a trapezoidal enclosure using Cu–water nanofluid. Comput. Fluids 72, 46–62.

Majeed, A., Javed, T., Mustafa, I., 2016. Heat transfer analysis of boundary layer flow over hyperbolic stretching cylinder. Alexandria Eng. J. 55, 1333–1339.

Mansour, M.A., Mohamed, R.A., Abd-Elaziz, M.M., Ahmed, S.E., 2011. Thermal stratification and suction/injection effects on flow and heat transfer of micropolar fluid due to stretching cylinder. Int. J. Numer. Methods Biomed. Eng. 27 (12), 1951–1963. http://dx.doi.org/10.1002/cnm.1449.

Mansour, M.A., Ahmed, S.E., Aly, A.M., Rashad, A.M., 2016. MHD effects on entropy generation and heat transfer of nanofluid flows in enclosures. J. Nanofluids 5, 595–605.

Mchirgui, A., Hidouri, N., Magherbi, M., Ben Brahim, A., 2012. Entropy generation in double-diffusive convection in a square porous cavity using Darcy-Brinkman formulation. Transp. Porous Media 93, 223–240.

Mehrez, Z., Bouterra, M., El Cafsi, A., Belghith, A., 2013. Heat transfer and entropy generation analysis of nanofluids flow in an open cavity. Comput. Fluids 88, 363–373.

Mukhopadhyay, S., 2012. Mixed convection boundary layer flow along a stretching cylinder in porous medium. J. Pet. Sci. Eng. 96–97, 73–78.

Mukhopadhyay, S., 2013. MHD boundary layer slip flow along a stretching cylinder. Ain Shams Eng. J. 4, 317–324.

Nayak, R.K., Bhattacharyya, S., Pop, I., 2016. Heat transfer and entropy generation in mixed convection of a nanofluid within an inclined skewed cavity. Int. J. Heat Mass Transfer 102, 596–609.

Nield, D.A., Kuznetsov, A.V., 2009. The Cheng-Minkowycz problem for natural convective boundary-layer flow in a porous medium saturated by a nanofluid. Int. J. Heat Mass Transfer 52, 5792–5795.

Noghrehabadi, A., Saffarian, M.R., Pourrajab, R., Ghalambaz, M., 2013. Entropy analysis for nanofluid flow over a stretching sheet in the presence of heat generation/absorption and partial slip. J. Mech. Sci. Technol. 27 (3), 927–937.

Parvin, S., Nasrin, R., Alim, M.A., 2014. Heat transfer and entropy generation through nanofluid filled direct absorption solar collector. Int. J. Heat Mass Transfer 71, 386–395.

Rashad, A.M., Chamkha, A.J., Modather, M., 2013. Mixed convection boundary-layer flow past a horizontal circular cylinder embedded in a porous medium filled with a nanofluid under convective boundary condition. Comput. Fluids 86, 380–388.

Rashidi, M.M., Parsa, A.B., Shamekhi, L., Momoniat, E., 2015. Entropy generation analysis of the revised cheng-minkowycz problem for natural convective boundary layer flow of nanofluid in a porous medium. Therm. Sci. 19, S169–S178. Suppl. 1.

Shahi, M., Mahmoudi, A.H., Raouf, A.H., 2011. Entropy generation due to natural convection cooling of a nanofluid. Int. Commun. Heat Mass Transfer 38, 972–983.

Shehzad, N., Zeeshan, A., Ellahi, R., Vafai, K., 2016. Convective heat transfer of nanofluid in a wavy channel: Buongiorno's mathematical model. J. Mol. Liq. 222, 446–455.
Sheikholeslami, M., 2017. Influence of magnetic field on nanofluid free convection in an open porous cavity by means of Lattice Boltzmann method. J. Mol. Liq. 234, 364–374.
Sheikholeslami, M., Bhatti, M.M., 2017. Active method for nanofluid heat transfer enhancement by means of EHD. Int. J. Heat Mass Transfer 109, 115–122.
Sheikholeslami, M., Rokni, H.B., 2017. Nanofluid two phase model analysis in existence of induced magnetic field. Int. J. Heat Mass Transfer 107, 288–299.
Sheikholeslami, M., Sadoughi, M., 2017. Mesoscopic method for MHD nanofluid flow inside a porous cavity considering various shapes of nanoparticles. Int. J. Heat Mass Transfer 113, 106–114.
Sheikholeslami, M., Shehzad, S.A., 2017a. Thermal radiation of ferrofluid in existence of Lorentz forces considering variable viscosity. Int. J. Heat Mass Transfer 109, 82–92.
Sheikholeslami, M., Shehzad, S.A., 2017b. Magnetohydrodynamic nanofluid convection in a porous enclosure considering heat flux boundary condition. Int. J. Heat Mass Transfer 106, 1261–1269.
Sheikholeslami, M., Zeeshan, A., 2017. Analysis of flow and heat transfer in water based nanofluid due to magnetic field in a porous enclosure with constant heat flux using CVFEM. Comput. Methods Appl. Mech. Eng. 320, 68–81.
Wang, C., 1988. Fluid flow due to a stretching cylinder. Phys. Fluids 31, 466–468.
Zeeshan, A., Majeed, A., 2016. Non-Darcy mixed convection flow of magnetic fluid over a permeable stretching sheet with Ohmic dissipation. J. Mag. 21 (1), 153–158.
Zeeshan, A., Majeed, A., Ellahi, R., 2016. Effect of magnetic dipole on viscous ferrofluid past a stretching surface with thermal radiation. J. Mol. Liq. 215, 549–554.
Zeeshan, A., Hassan, M., Ellahi, R., Nawaz, M., 2016. Shape effect of nanosize particles in unsteady mixed convection flow of nanofluid over disk with entropy generation. Proc. Inst. Mech. Eng., Part E: J. Process Mech. Eng. 0954408916646139.